Volume 52
Number 21
7 June 2023
Pages 6947-7356

Dalton Transactions

An international journal of inorganic chemistry

rsc.li/dalton



ISSN 1477-9226

ROYAL SOCIETY OF CHEMISTRY

PAPER

Zehra Altuntaş Bayır *et al.*

The effect of phthalocyanine's periphery on the biological activities of carbazole-containing metal phthalocyanines

Dalton Transactions

ROYAL SOCIETY OF CHEMISTRY

PAPER

Check for updates

Cite this: *Dalton Trans.*, 2023, **52**, 7009

The effect of phthalocyanine's periphery on the biological activities of carbazole-containing metal phthalocyanines

Nazli Farajzadeh, [a] H. Yasemin Yenilmez,[a] Dilek Bahar,[b] Nilgün Güler Kuşçulu,[c] Emine Kılıçkaya Selvi[c] and Zehra Altuntaş Bayır *[a]

Received 27th February 2023,
Accepted 9th April 2023

DOI: 10.1039/d3dt00615h

rsc.li/dalton

This study reports the synthesis and characterization of two new mono- and di-substituted phthalonitriles namely 4-((9*H*-carbazol-3-yl)oxy)-5-chlorophthalonitrile and 4,5-bis((9*H*-carbazol-3-yl)oxy)phthalonitrile, respectively. Cyclotetramerization of the new phthalonitriles in the presence of zinc(II) acetate resulted in related zinc(II) phthalocyanines. To study the effect of the position and number of substituents on the biological properties of the phthalocyanines, peripherally or non-peripherally tetra-substituted zinc(II) phthalocyanines bearing (9*H*-carbazol-3-yl)oxy groups, as well as axially di-substituted silicon phthalocyanines containing the same groups, were prepared. Since gold nanoparticles are well-known as efficient drug delivery agents, the surface of these metal nanoparticles was functionalized with all the compounds. This modification also improved the solubility of the phthalocyanines in aqueous media. In this study, the antioxidant, DNA cleavage, and toxic/phototoxic activities of the resultant nanoconjugates were examined. With a combination of metal ion and substituent (nature, number, and position) effects, the silicon(IV) phthalocyanine exhibited the highest biological properties.

Introduction

Carbazole is a nitrogen-containing tricyclic system that is well-known as an essential structure of synthetic and natural biologically active materials.[1] Although these heterocyclic structures are similar to those of cyclic organic hydrocarbons, they can exhibit different properties from their hydrocarbon analogs. Generally, the identity, number, and location of heteroatoms are vital factors that result in various physical and biological features. There are a number of studies reporting different biological properties of carbazoles. Antibacterial, anti-cancer, antifungal, anti-HIV, anti-inflammatory, anti-protozoan, and hepatoprotective activities are biological characteristics that have been examined for carbazole-based compounds.[2–6] A wide range of synthetic drugs contain a carbazole-based nucleus as a pharmacophore system playing a vital role in the binding of the drug to the target structure. Due to the immense potential of the carbazole derivatives, their therapeutic properties have attracted attention for the design of new efficient mitigated drugs in recent years. Benzocarbazoles,[7] furo-carbazoles,[8] imidazocarbazoles,[9] indolocarbazoles,[10] oxazinocarbazoles, pyrido-carbazolequinone,[11] pyridocarbazoles,[12] tetrahydrocarbazoles,[13] and thiazolocarbazoles[14] are a number of carbazole derivatives that display high medical activities.[15] Additionally, some studies have reported the biological features of carbazole-containing metal phthalocyanines.[16–18]

Phthalocyanines are one of the common porphyrin analogs that consist of an extensive two-dimensional π-system. High electron transfers arising from their π-conjugated structure result in excellent biological, chemical, electronic, and optical properties.[19,20] However, the lack of sufficient solubility in common organic or aqueous media resulting from strong π-stacking interactions is an obstacle to their use in many scientific and high-tech fields. The structural flexibility of the phthalocyanine ring makes possible the insertion of metal ions into the phthalocyanine center and/or the addition of various substituents to the phthalocyanine ring.[21–26] These architectural changes decrease the intermolecular interactions and improve solubility. The presence of metal cations and substituents alters the characteristic properties of phthalocyanines, as well.[27–30] Phthalocyanines have also been used for the modification of gold nanoparticles in recent years. Obaid *et al.* modified the surface of gold nanoparticles with 1,1′,4,4′,8,8′,15,15′,18,18′,22,22′-tetradecakisdecyl-25,25′-(11,11′

[a]*Department of Chemistry, Istanbul Technical University, TR-34469 Istanbul, Türkiye. E-mail: bayir@itu.edu.tr*
[b]*Genome & Stem Cell Center (GENKOK), Erciyes University, TR-38280 Kayseri, Türkiye*
[c]*Department of Chemistry Technology, Mustafa Çıkrıkçıoğlu Vocational School, Kayseri University, TR-38280 Kayseri, Türkiye*

This journal is © The Royal Society of Chemistry 2023

dithiodiundecyl) diphthalocyanine zinc (C11Pc) and lectin jacalin and investigated their photodynamic therapeutic activity against HT-29 human colorectal adenocarcinoma cells. The nanoconjugates exhibited higher activity upon irradiation compared with unmodified gold nanoparticles.[31] Stuchinskaya *et al.* designed 4-component gold nanoparticles conjugated with C11Pc and studied their potential as a photodynamic cancer therapeutic drug for the treatment of breast cancer cells. The resultant nanoconjugates attack selectively the cancer lesions.[32]

The optical properties of gold nanoparticles have extensively attracted attention for many years since the increase in the ratio of surface-to-volume results in unique characteristics of nano-sized materials that are not introduced in their bulk forms.[33] Also, the inert and non-toxic nature, ease of size control and surface modification, and monodispersity of gold nanoparticles are essential factors for their potent utility as suitable biological agents. These metallic nanoparticles have been well-known as strong delivery candidates for various compounds ranging from small molecules to large biomolecules in the cells.[34] The encapsulation or incorporation of therapeutic compounds on gold nanoparticles can be carried out through surface conjugation or surface adsorption.[35] The surface of gold nanoparticles has been modified with various compounds consisting of peptides, polymers, phthalocyanines, DNAs, and rhodamines.[36,37] The conjugation of gold nanoparticles and phthalocyanines results in the combination of their extraordinary properties which, in turn, can promise the design of efficient nanoconjugates for scientific applications. Phthalocyanines mostly link to the surface of gold nanoparticles through Au–N bonds,[38] Au–S bonds,[39] or electrostatic interactions.[40] They assemble on the surface of gold nanoparticles and form a monolayer.[41]

Some biochemicals (enzymes, metalloproteins, metals, and microorganisms) and physical parameters (heat and light) play a vital role in lipid oxidation that, in turn, deteriorates food quality.[42] Additionally, lipids are normally oxidized in living cells during aerobic metabolisms. However, the occurrence of lipid oxidation in the presence of unsaturated fatty acids irreversibly results in cellular damage.[43] Autoxidation, enzymatic oxidation, thermal oxidation, and photooxidation of lipids include some reactive intermediate species such as free radicals. Therefore, the inactivation of these species significantly prevents oxidative deterioration in biological systems and foods.[44] Antioxidants inhibit oxidation processes, promote the efficiency of nutritional drugs (dietary supplements and nutraceuticals), and lead to food preservation and good body health.[45,46] Gold is a diamagnetic metal in the block state; however, gold nanoparticles exhibit ferromagnetic spin polarization since the electronic structure of the metal can change by decreasing the particle size. In the literature, some studies report the antioxidant activities of gold nanoparticles against hydroxyl radicals.[47] On the other hand, metal phthalocyanines display high antioxidant activities against different microorganisms.[48] Therefore, the modification of the surface of gold nanoparticles with metal phthalocyanines can improve their individual properties. The antioxidant properties of phthalocyanine–gold nanoconjugates have been included in our previous studies for the first time.[49,50]

The interaction of compounds with DNA molecules is mostly studied to examine the potent activities of new drugs and biological systems that can be utilized for cancer treatments.[51] Cancer is an uncontrolled expansion of cells that leads to remarkable human deaths all over the world. Therefore, the prevention of cell division depending on their DNA replication is an efficient way to control or fight cancer. The linkages of organic or inorganic compounds to DNA molecules can lead to the breaking of DNAs which is responsible for the transfer of the codes of disorders.[52] Organic/inorganic compounds can interact covalently or non-covalently with DNA molecules. The compounds non-covalently interacting with DNAs link to these molecules through electrostatic interactions, minor groove binding, or intercalation.[53–56] Although gold nanoparticles do not exhibit any interactions with DNAs, modification of their surface with suitable compounds can improve their interactions. Our group has studied the DNA interaction of phthalocyanine–gold nanoconjugates for the first time.[49,50]

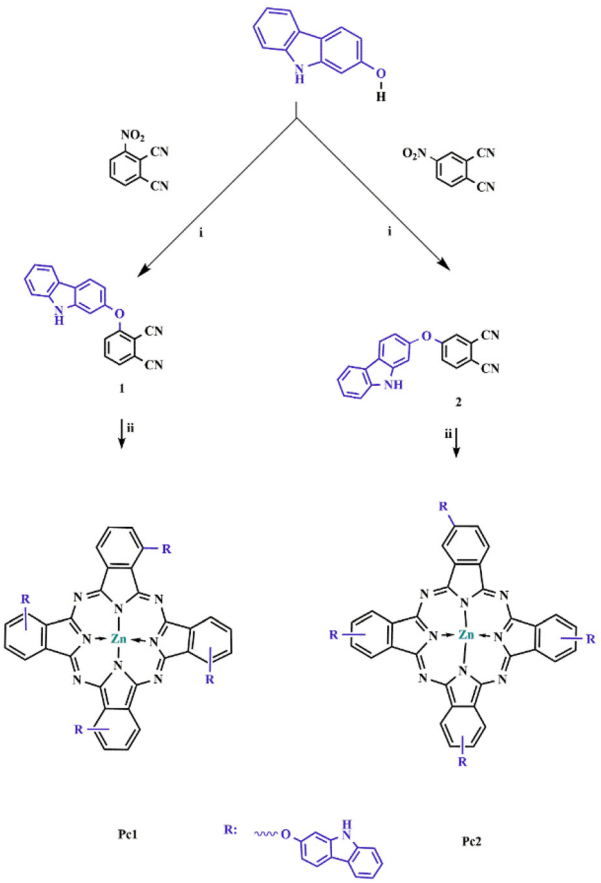
This study aims to design efficient biochemical antioxidants and anticancer agents. Carbazole is a potent antineoplastic compound exhibiting high biological activities as well as gold nanoparticles and phthalocyanines. On the other hand, the number and position of substituents can affect the chemical and biological properties of phthalocyanines. Hence, a series of peripherally/non-peripherally tetra-, peripherally octa-, and axially substituted metal phthalocyanines bearing chlorine and/or carbazole groups were prepared and characterized. To combine the biological features of carbazole, phthalocyanine, and gold nanoparticles, the resultant carbazole-containing metal phthalocyanines were used for the modification of the gold nanoparticle surface for the first time. The singlet oxygen production capacity of the nanoconjugates was evaluated. Also, their DNA cleavage, antioxidant, and cytotoxic properties were investigated using the agarose gel, 2,2-diphenyl-1-picrylhydrazyl (DPPH), and 3-[4,5-dimethylthiazole-2-yl]-2,5-diphenyltetrazolium bromide (MTT) assays.

Results and discussion

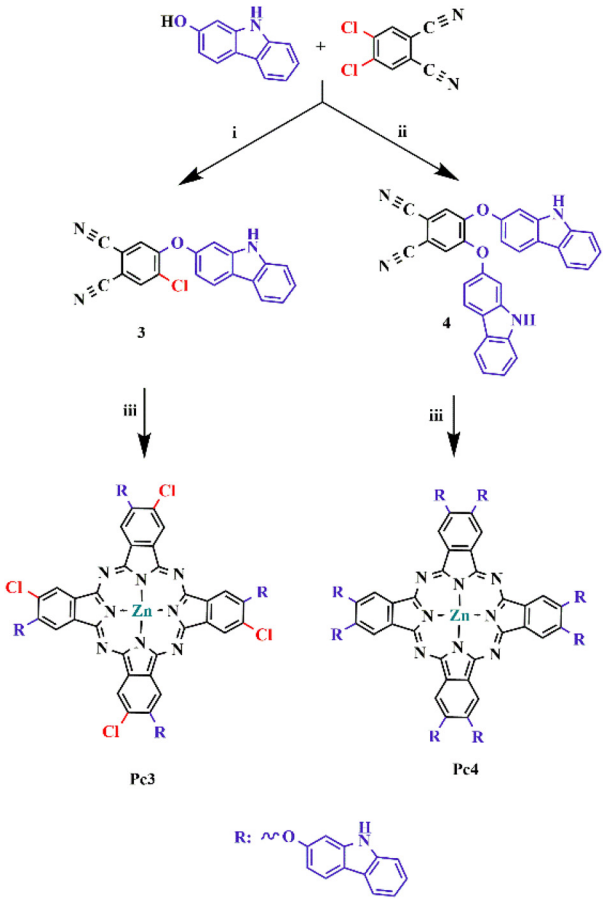
Synthesis

Compounds **1**, **2**, **Pc1**, and **Pc2** were synthesized as described in ref. 57 and 58 with some modifications (Scheme 1). New phthalonitrile derivatives **3** and **4** were prepared by using the combination of 9*H*-carbazol-3-ol and 4,5-dichlorophthalonitrile through the nucleophilic substitution reaction (Scheme 2). Characterization of the resultant compounds was carried out by performing ^{1}H NMR, ^{13}C NMR, and FT-IR spectroscopy. In the ^{1}H NMR spectra of compounds **3** and **4**, the respective protons of amine appeared at 11.42 and 11.43 ppm as singlets assigned to 1H and 2H. The respective phthalonitrile aromatic protons of compound **3** were observed at 8.56

 This journal is © The Royal Society of Chemistry 2023



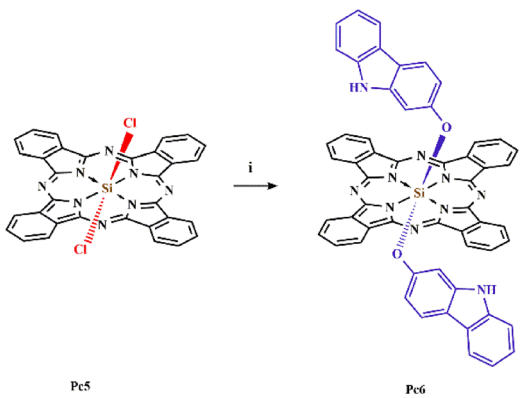
Scheme 1 The synthetic procedures for compounds (**1**, **2**, **Pc1** and **Pc2**). (i) K_2CO_3 and dimethylformamide (DMF); (ii) $Zn(CH_3COO)_2$ and DMAE.



Scheme 2 The synthetic procedures for compounds (**3**, **4**, **Pc3** and **Pc4**). (i) and (ii) are identical: K_2CO_3 and dimethyl sulfoxide (DMSO); (iii) $Zn(CH_3COO)_2$ and *N*,*N*-dimethylaminoethanol (DMAE).

and 7.61 ppm as singlets corresponding to Ar–H–O and Ar–H–Cl, whereas those of compound **4** were observed at 8.57 ppm as a singlet assigned to 2H. In the ^{1}H NMR spectra of compounds **3** and **4**, the carbazole aromatic protons appeared between 8.22 and 6.95 ppm. In the ^{13}C NMR spectra, the carbon signals of compound **3** appeared between 158.03 and 102.87 ppm whereas those of compound **4** were observed between 158.03 and 102.90 ppm. The carbon signals of the nitrile groups of compounds **3** and **4** appeared at 115.51–115.40 and 115.38 ppm, respectively. In the FT-IR spectrum of compound **3**, the bands appeared at 3406, 3078, 2238, and 1120 cm^{-1} corresponded to N–H, aromatic C–H, nitrile, and C–O–C vibrations, respectively. In the FT-IR spectrum of compound **4**, the N–H, aromatic C–H, nitrile, and C–O–C vibrations were observed at 3394, 3055, 2236, and 1118 cm^{-1}, respectively.

The cyclotetramerization of compounds **3** and **4** resulted in macromolecules **Pc3** and **Pc4** in the presence of zinc acetate (Scheme 2). Besides, 9*H*-carbazol-3-ol was replaced with chlorine atoms of silicon(IV) phthalocyanine dichloride (**Pc5**) in the presence of NaH as a strong base which resulted in the formation of macromolecule **Pc6** (Scheme 3). The newly synthesized compounds were characterized using a number of



Scheme 3 The synthetic procedures for compound **Pc6**, (i) NaH and toluene.

diverse spectroscopic methods such as ^{1}H NMR, mass, and FT-IR spectroscopy. In the related ^{1}H NMR spectra, the N–H signals of compound **Pc3** appeared between 11.39 and 11.17 ppm as multiplets whereas those of macromolecules **Pc4** and **Pc6** were observed at 11.40 and 11.91 ppm as singlets. In the FT-IR spectra of the newly synthesized phthalocyanines,

the cyclotetramerization of the related phthalonitrile derivatives led to the disappearance of the nitrile bands. Also, the N–H vibrations appeared at around 3400 cm^{-1} whereas the aromatic C–H bands were observed between 3051 and 3063 cm^{-1}. The respective C–O–C vibrations of macromolecules **Pc3** and **Pc4** were observed at 1119 and 1116 cm^{-1}. In the MALDI-TOF spectra of macromolecules **Pc3**, **Pc4**, and **Pc6**, the molecular ion peaks appeared at 1436.65, 2074.52, and 558.16 *m*/*z* and were assigned to $[M - 4H]^+$, $[M + 2Na + H]^+$, and $[M + CHCA + H]^{2+}$, respectively. All the obtained data were in accordance with the target structures. The UV-vis spectra of macromolecules (**Pc1-6**) were recorded in DMSO at room temperature. The data of the electronic absorption spectra of **Pc1-6** and **Au-Pc1-6** are summarized in Table 1. The conjugation of the compounds (**Pc1-6**) to the gold nanoparticles' surface led to the blue-shift of their electronic absorption spectra.

The transmission electron microscopic technique was applied for the characterization of the gold nanoparticles (AuNPs) and nanoconjugates (**Au-Pc1-6**). The TEM analysis was carried out at the Middle East Technical University and the related images are illustrated in Fig. 1. Fig. 1a demonstrates well-dispersed spherical gold nanoparticles. The conjugation of the gold nanoparticles with the compounds (**Pc1-6**) resulted in aggregation and a considerable decrease in the distance between the spherical particles (Fig. 1b–g). The size of unmodified gold nanoparticles was found to be approximately 15 nm and enhanced by functionalization of the surface with the phthalocyanines owing to H-aggregates originating from the π–π interaction between the modified phthalocyanines.[59,60] Additionally, the agglomeration of gold nanoparticles conjugated to the phthalocyanines led to the approach/association of the particles. The modified gold nanoparticles were determined to be between 20 and 23 nm in size.

Table 1 The data of the electronic absorption spectra of **Pc1-6** and **Au-Pc1-6**

Compound	λ_{max} of B-band/nm (log ε)	λ_{max} of Q-band/nm (log ε)
Pc1	328 (4.41)	702 (4.92)
Pc2	334 (4.49)	684 (4.87)
Pc3	332 (4.64)	685 (4.94)
Pc4	329 (4.90)	685 (4.76)
Pc5	330 (4.61)	676 (4.94)
Pc6	327 (5.00)	682 (4.64)
Au-Pc1	332 (4.36)	700 (5.02)
Au-Pc2	331 (4.61)	682 (4.92)
Au-Pc3	330 (4.66)	683 (4.99)
Au-Pc4	326 (5.00)	682 (4.82)
Au-Pc5	328 (4.65)	672 (4.92)
Au-Pc6	324 (5.02)	680 (4.80)

Singlet oxygen quantum yield (φ_Δ)

Generally, the singlet oxygen production capacity of a photosensitizing agent is evaluated to measure its potent utility for photodynamic therapeutic applications.[61] In this study, the singlet oxygen quantum yields of the nanoconjugates (**Au-Pc1-6**) were determined in DMSO using the phosphorescence signal of singlet oxygen at 1270 nm.[62] The results are summarized in Table 2. The highest value was obtained for nanoconjugate **Au-Pc6**. Although the singlet oxygen quantum yields of the nanoconjugates (**Au-Pc4** and **Au-Pc5**) were found to be lower than the standard (ZnPc; φ_Δ = 0.67 in DMSO), their singlet oxygen quantum yields were sufficient for photodynamic therapy compared with the literature.[41,63] Therefore, all the nanoconjugates can be used as efficient photosensitizers for photodynamic therapy (PDT) after further investigations.

Antioxidant properties

The 2,2-diphenyl-1-picrylhydrazyl scavenging activities of the nanoconjugates (**Au-Pc1-6**) were studied using trolox as the

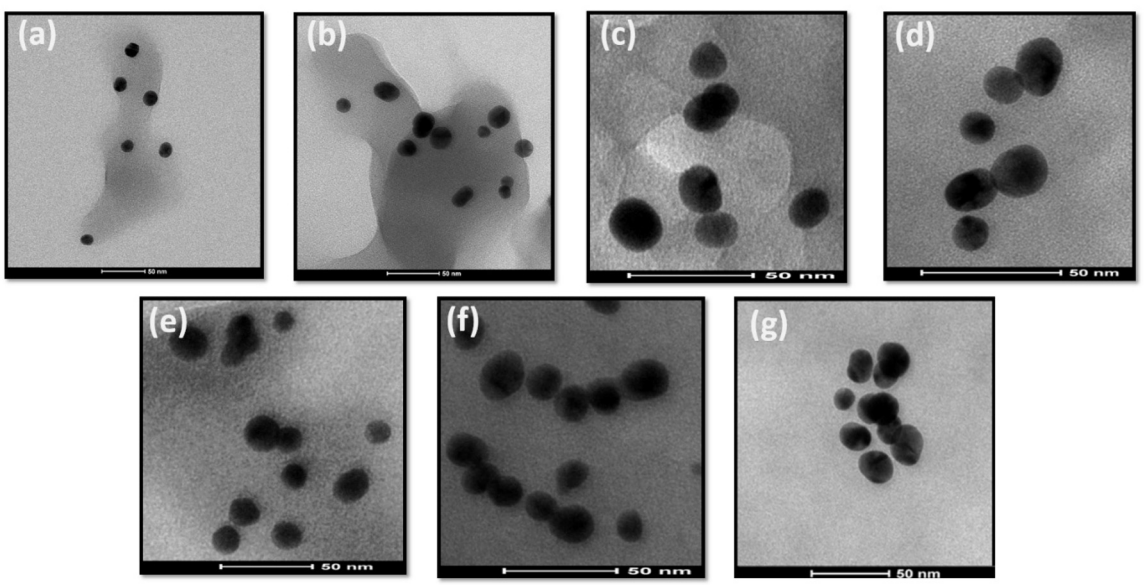


Fig. 1 TEM images of nanoconjugates. (a) **AuNPs**; (b) **Au-Pc1**; (c) **Au-Pc2**; (d) **Au-Pc3**; (e) **Au-Pc4**; (f) **Au-Pc5**; (g) **Au-Pc6**.

 This journal is © The Royal Society of Chemistry 2023

Table 2 The singlet oxygen quantum yields of nanoconjugates (**Au-Pc1-6**)

Nanoconjugate	Singlet oxygen quantum yield (φ_Δ)
Au-Pc1	0.75
Au-Pc2	0.81
Au-Pc3	0.85
Au-Pc4	0.54
Au-Pc5	0.40
Au-Pc6	0.92

representative standard (SC_{50} = 0.001 ± 0.000 mg mL^{-1}) (Fig. 2). The determined SC_{50} values are summarized in Table 3. The SC_{50} values of the nanoconjugates ranged from 0.003 ± 0.000 to 0.078 ± 0.016 mg mL^{-1}. Although all the nanoconjugates exhibited high DPPH radical scavenging activities, the highest activity was obtained for nanoconjugate **Au-Pc6** (SC_{50} = 0.003 ± 0.000 mg mL^{-1}) and its SC_{50} value was so closer to that of Trolox. However, the lowest scavenging activity was obtained for nanoconjugate **Au-Pc1** (SC_{50} = 0.078 ± 0.016 mg mL^{-1}). As a result, the presence of carbazole groups in peripheral positions improved the antioxidant activities of the phthalocyanines compared to the presence of the same groups in non-peripheral positions. Also, an increase in the number of substituents was followed by the refinement of the antioxidant activities. The presence of chlorine atoms on the

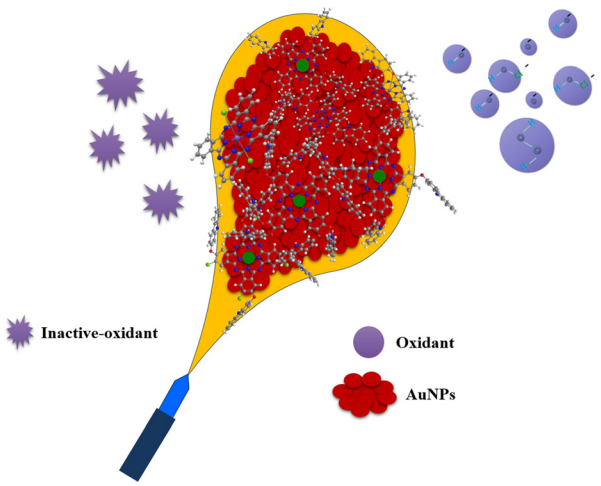


Fig. 2 The general antioxidant activity of nanoconjugates (**Au-Pc1-6**).

Table 3 DPPH radical scavenging activities of nanoconjugates (**Au-Pc1-6**)

Nanoconjugate	DPPH method (SC_{50} value, mg mL^{-1})
Au-Pc1	0.078 ± 0.016
Au-Pc2	0.034 ± 0.011
Au-Pc3	0.046 ± 0.008
Au-Pc4	0.028 ± 0.005
Au-Pc5	0.015 ± 0.003
Au-Pc6	0.003 ± 0.000
Trolox	0.001 ± 0.000

periphery of the phthalocyanine ring weakened its activity. There are some similar studies in the literature. Alici *et al.* studied the antioxidant properties of non-peripherally and peripherally substituted metal-free, zinc, and cobalt phthalocyanines bearing 4-methoxy-phenoxy groups. The non-peripherally- substituted zinc phthalocyanine did not exhibit antioxidant properties whereas its peripherally-substituted analog exhibited high activity.[64] Salehi and Karimi examined the antioxidant properties of the newly synthesized metal phthalocyanines [M: Co(II), Cu(II), Zn(II), Mn(II)] bearing eight peripheral 2,6-di-tert-buthyl-phenol groups. All the nanoconjugates exhibited good activities.[65] Çelik *et al.* synthesized new symmetric and unsymmetric axially di-substituted silicon phthalocyanines and examined their antioxidant properties. Symmetric silicon phthalocyanines bearing diclofenac groups in the axial positions displayed higher antioxidant activity.[66] Compared with the literature, the nanoconjugates (**Au-Pc1-6**) exhibited high antioxidant activities and can be used as suitable antioxidants after further investigations.

DNA cleavage studies

The DNA cleavage properties of the nanoconjugates (**Au-Pc1-6**) and gold nanoparticles (**AuNPs**) were evaluated using an agarose gel method. The obtained results are demonstrated in Fig. 3. All the nanoconjugates cleaved the DNA molecules and led to the formation of Form II at the studied concentrations. Nanoconjugate **Au-Pc5** exhibited higher DNA cleavage activities since it resulted in the formation of Form III at all the studied concentrations. The DNA converted to Form III in the presence of 5 mg mL^{-1} nanoconjugate **Au-Pc6** whereas it formed Form III in the presence of 2.5 mg mL^{-1} nanoconjugates (**Pc1**, **Pc2**, and **Pc4**). The DNA cleavage activity of the non-peripherally tetra-substituted zinc phthalocyanine was approximately similar to the DNA cleavage activities of the peripherally tetra- and octa-substituted analogs. However, these activities were weaker than those of the axially di-substituted silicon(IV) phthalocyanines. Therefore, the presence of the ligands at the axial positions improved the DNA cleavage. Additionally, the carbazole group was more effective than the chlorine atom. Gold nanoparticles (**AuNPs**) did not exhibit any DNA cleavage activity.[67] As a result, the modification of the gold nanoparticles' surface with the compounds (**Pc1-6**) improved their DNA cleavage activities. Some similar studies have been reported in the literature. Barut *et al.* prepared tetra-substituted zinc(II) phthalocyanines bearing 2-(piperidin-1-yl) phenoxy groups at peripheral or non-peripheral positions. The peripherally tetra-substituted zinc(II) phthalocyanine exhibited better DNA cleavage activity than its non-peripheral analogs.[68] Çelik *et al.* synthesized a series of axially symmetric and di-substituted silicon(IV) phthalocyanines bearing meloxicam, triethylene glycol monomethyl ether, or diclofenac units. The silicon(IV) phthalocyanine containing different ligands at the axial positions led to the conversion of Form I to Form III at the studied concentrations. Compared to the literature, all the studied nanoconjugates exhibited acceptable DNA cleavage activities.[66]

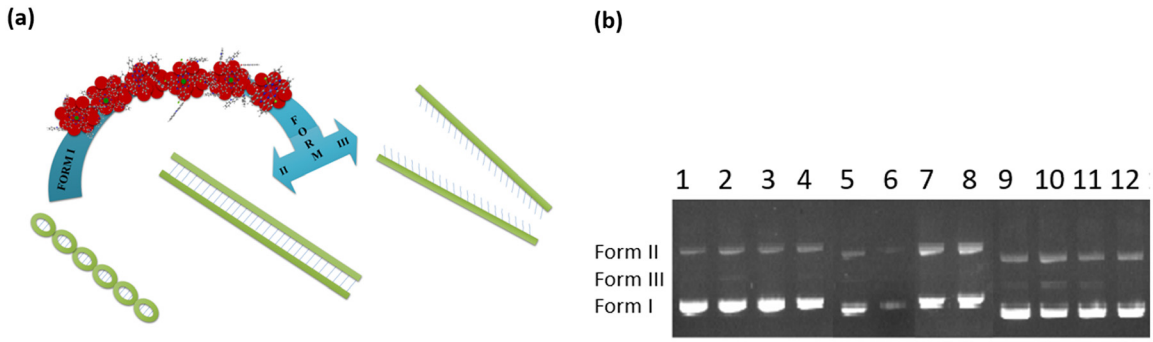


Fig. 3 (a) The general DNA cleavage activity of nanoconjugates (**Au-Pc1-6**); (b) DNA cleavage activity of nanoconjugates (**Au-Pc1-6**) after 24 hours of incubation. Lane (**1**) pBR 322DNA + 5 mg mL^{-1} of **Au-Pc1** + ddw. Lane (**2**) pBR 322DNA + 2.5mg mL^{-1} of **Au-Pc1** + ddw. Lane (**3**) pBR 322DNA + 5mg mL^{-1} of **Au-Pc2** + ddw. Lane (**4**) pBR 322DNA + 2.5 mg mL^{-1} of **Au-Pc2** + ddw. Lane (**5**) pBR 322DNA + 5 mg mL^{-1} of **Au-Pc3** + ddw. Lane (**6**) pBR 322DNA + 2.5 mg mL^{-1} of **Au-Pc3** + ddw. Lane (**7**) pBR 322DNA + 5 mg mL^{-1} of **Au-Pc4** + ddw. Lane (**8**) pBR 322DNA + 2.5 mg mL^{-1} of **Au-Pc4** + ddw. Lane (**9**) pBR322DNA + 5 mg mL^{-1} of **Au-Pc5** + ddw. Lane (**10**) pBR322DNA + 2.5 mg mL^{-1} of **Au-Pc5** + ddw. Lane(**11**) pBR322DNA + 5 mg mL^{-1} of **Au-Pc6** + ddw. Lane (**12**) pBR322DNA + 2.5 mg mL^{-1} of **Au-Pc6** + ddw.

Cell culture

In this study, the DLD-1 and HepG2 cell lines were cultured without any contamination. The control group cells maintained the original morphology during culture; however, the incubation of the cells with the nanoconjugates (**Au-Pc1-6**) led to the shrinkage of the structure and an abnormal morphology (Fig. 4).

MTT assay

The cytotoxic activities of the nanoconjugates (**Au-Pc1-6**) against the studied cell lines were examined using *in vitro* MTT assays (Fig. 4). The obtained results are listed in Tables 4 and 5. The proliferative activities of the nanoconjugates (**Au-Pc1-6**) were tested against two human cancer cell lines (DLD-1 and HepG2). The cell lines were incubated with different concentrations of the nanoconjugates (**Au-Pc1-6**) for 24 hours under normal and white light irradiation. Cisplatin was used as a positive control. The obtained results confirmed that all the nanoconjugates exhibited a negative effect on cell proliferation in a dose-dependent manner. Nanoconjugate **Au-Pc6** displayed the highest activity against the DLD-1 cell line under white lamp irradiation (IC_{50} = 11.87 μM). Also, the lowest IC_{50} of 25 μM was obtained against the HepG2 cell line for nanoconjugate **Au-Pc6** in the dark and under white irradiation. The cytotoxic results of the nanoconjugates (**Au-Pc1-6**) are demonstrated in Fig. 5 and 6.

DLD-1

Fig. 5 shows cell proliferation (%) at different concentrations of the nanoconjugates (**Au-Pc1-6**) with and without white lamp irradiation on the DLD-1 cell line. The calculated IC_{50} values are listed in Table 4. As the concentration of the nanoconjugates (**Au-Pc1-6**) increased, the cell proliferation decreased. Compared to Cisplatin, 200 μM nanoconjugates **Au-Pc5** and **Au-Pc6** exhibited statistically different behavior in the dark (**PAu-Pc5**-CisPt = 0.02; **PAuPc6**-CisPt = 0.01) and under white light irradiation (**PAuPc5**-CisPt = 0.00; **PAuPc6**-CisPt = 0.02). Moreover, there were statistical differences between the dark and the white light irradiation groups for **Au-Pc2** (P25 μM = 0.01 and P12.5 μM = 0.03), **Au-Pc3** (P12.5μM = 0.04), and **Au-Pc5** (P200 μM = 0.05 and P25 μM = 0.02). Ozdemir *et al.* prepared tetra-substituted zinc(II) and indium(III) chloride phthalocyanines bearing bis(trimethylsilyl)amine units at peripheral and non-peripheral positions. Their apoptotic, cytotoxic, and genotoxic activities against colon cancer (LoVo cell lines) were investigated. The non-peripherally substituted zinc phthalocyanine displayed the highest apoptotic, cytotoxic, and genotoxic effects on the LoVo cell lines.[69] Nkune *et al.* studied the photosensitizing properties of zinc phthalocyanine tetrasulfonic acid and its gold nanoconjugates using colorectal cancer (CRC) cells. All the compounds especially the nanoconjugates exhibited high activity.[70] In our previous study, the effect of the axial ligand length on the cytotoxicity/photocytotoxicity of the silicon(IV) phthalocyanines against DLD-1 cell lines was examined. Although the compounds displayed high activities with/without irradiation, the highest activity was obtained for the compound containing the longest axial length.[71]

HepG2

The changes in cell proliferation of the HepG2 cell line in the presence of different concentrations of the nanoconjugates (**Au-Pc1-6**) in the dark and under white lamp irradiation are portrayed in Fig. 6. The IC_{50} values are summarized in Table 5. The increase in the concentration of the nanoconjugates was followed by a decrease in the cell proliferation. Compared to Cisplatin, nanoconjugate **Au-Pc6** had a statistically different effect on the darkness group (**PAu-Pc6**-CisPt = 0.00) at 200 μM and 100 μM. However, nanoconjugates **Au-Pc5** and **Au-Pc6** exhibited statistically different properties (**PAu-Pc5**-CisPt = 0.00; **PAu-Pc6**-CisPt = 0.03) for the white light irradiation group at 200 μM concentration. Besides, there was a statistical difference between the dark and the white light irradiation groups in the presence of nanoconjugates **Au-Pc3** (P100 μM = 0.05), **Au-Pc5** (P12.5 μM = 0.00), and **Au-Pc6** (P200 μM = 0.01 and

This journal is © The Royal Society of Chemistry 2023

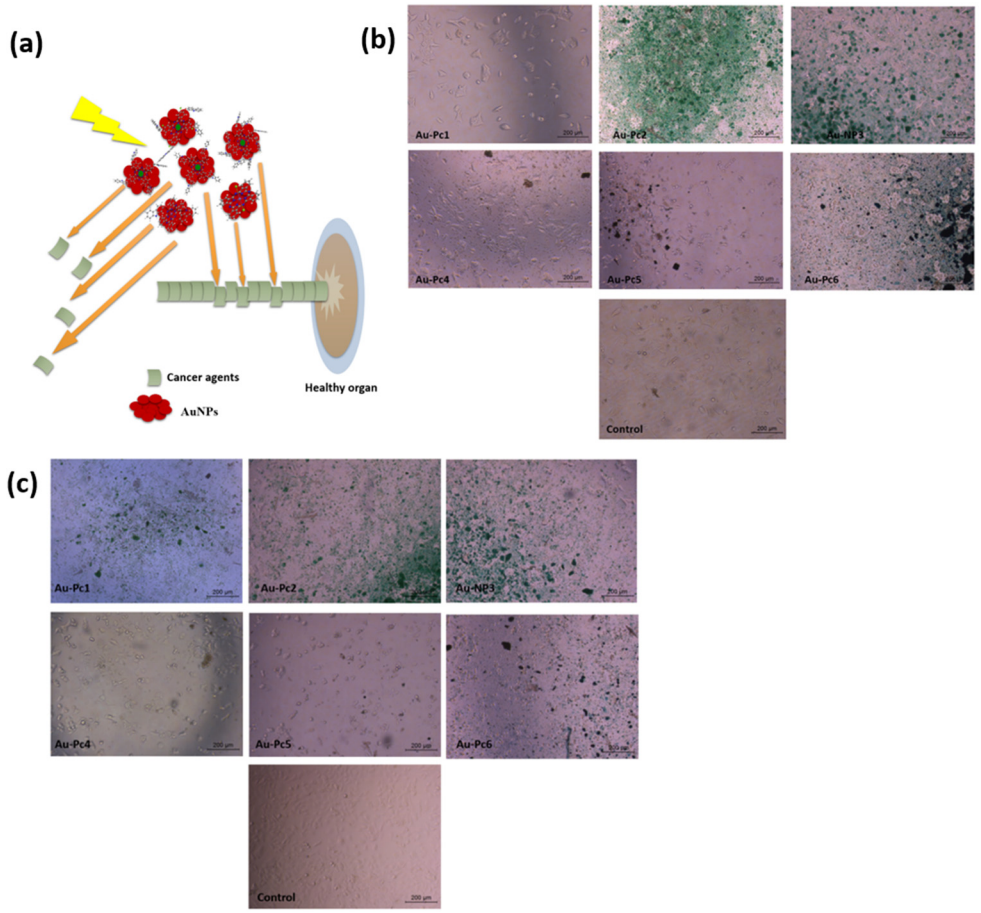


Fig. 4 (a) The general anticancer activity of nanoconjugates (**Au-Pc1-6**); (b) the microphotographs of the DLD-1 cells. Cell morphological character with 100 μM of each compound and control groups, for 24 hours, under inverted microscopy ×10; (c) the microphotographs of the HepG2 cells. Cell morphological character with 100 μM of each compound and control groups, for 24 hours, under inverted microscopy ×10.

Table 4 IC_{50} values of nanoconjugates (**Au-Pc1-6**) on the DLD-1 cell line

	IC_{50} values (μM)	
Nanoconjugate	Darkness group (without irradiation)	Photodynamic therapy group (white lamp irradiation)
Au-Pc1	228.61	200
Au-Pc2	200	108.23
Au-Pc3	237.1	106.75
Au-Pc4	240.63	233.48
Au-Pc5	58.682	25
Au-Pc6	47.227	12.5
AuNPs	248.49	81.513
Cisplatin	12.59	12.54

Table 5 IC_{50} values of nanoconjugates (**Au-Pc1-6**) on the HepG2 cell line

	IC_{50} values (μM)	
Nanoconjugate	Darkness group (without irradiation)	Photodynamic therapy group (white lamp irradiation)
Au-Pc1	106.66	100
Au-Pc2	50	43.841
Au-Pc3	180.48	53.264
Au-Pc4	219.88	100
Au-Pc5	45.952	50
Au-Pc6	25	96.155
AuNPs	100	100
Cisplatin	10.82	10.63

P100 μM = 0.01). Zhou *et al.* synthesized four mono-substituted zinc(II) phthalocyanines bearing coumarin units at peripheral or non-peripheral positions and examined their cytotoxic/photocytotoxic activities against HepG2. Although all the compounds exhibited higher activities, non-peripherally substituted zinc phthalocyanines mostly displayed better activities.[72] Sowa *et al.* prepared quaternized peripherally tetra- and octa-substituted zinc(II) phthalocyanines containing halogenated 7-hydroxycoumarin(umbelliferone) units and studied their phototoxic effects on HepG2 cells. An increase in the number of substituents led to higher phototoxicity.[73] Lo *et al.* synthesized some symmetric and unsymmetric axially di-substituted silicon(IV) phthalocyanines bearing 1,3-bis(dimethylamino) 2-propoxy group(s) and investigated their anticancer potency. All the compounds especially unsymmetric phthalocyanines exhibited high activities against HepG2.[74]

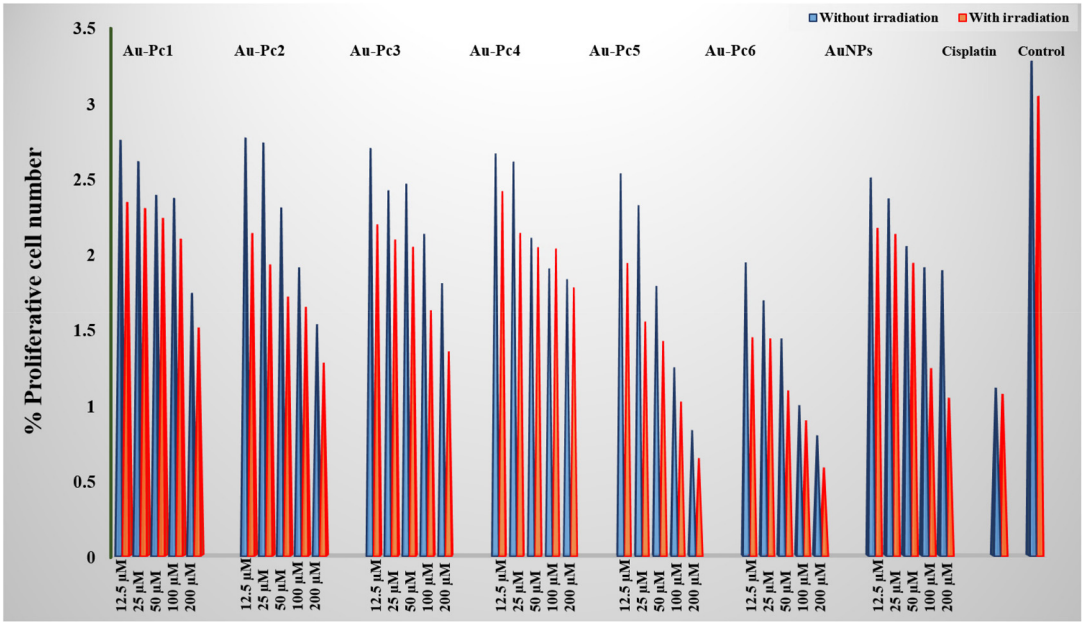


Fig. 5 Cell proliferation (%) at different concentrations of the nanoconjugates on the DLD-1 cell line, with and without white lamp irradiation. As nanoconjugate concentration increased, cell proliferation decreased.

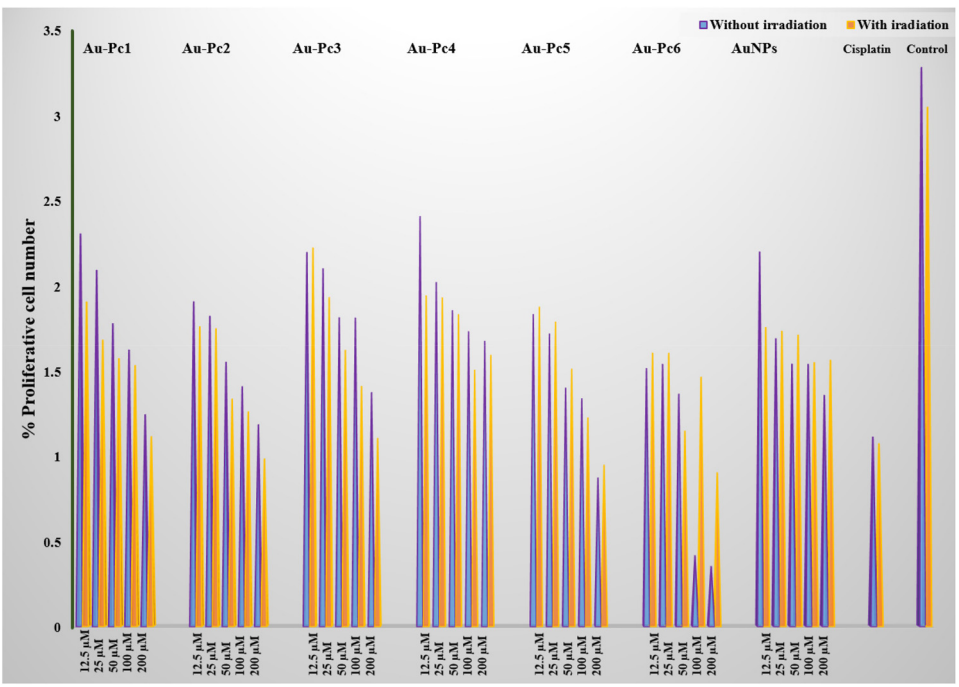


Fig. 6 Cell proliferation (%) at different concentrations of the nanoconjugates on the HepG-2 cell line, with and without white lamp irradiation. As nanoconjugate concentration increased, cell proliferation decreased.

Experimental

Materials

All the chemicals and solvents were purchased from commercial suppliers. They were of reagent-grade quality and consumed without any further purification. Silicon(IV) phthalocyanine dichloride (**Pc-5**) was obtained from Sigma Aldrich company.

Synthesis

3-(9*H*-Carbazol-2-yloxy)-phthalonitrile (**1**), 4-(9*H*-carbazol-2-yloxy)-phthalonitrile (**2**) and their zinc phthalocyanine deriva-

This journal is © The Royal Society of Chemistry 2023

tives (**Pc1** and **Pc2**) were synthesized as described in the literature with some modifications.[57,58]

General procedure for the synthesis of compounds (3 and 4)

4,5-dichlorophthalonitrile (1.00 g, 5.08 mmol) and 9*H*-carbazol-3-ol {(**3**: 0.930 g, 5.08 mmol); (**4**: 1.860 g, 10.16 mmol)} were dissolved in DMSO (15 mL). K_2CO_3 (3.51 g, 25.38 mmol) was added as the base catalyst. The reaction content was stirred for 48 hours under an inert atmosphere. The content was treated with the ice: water mixture (100 mL) and stirred for 1 hour. The pure product was recrystallized from ethanol.

4-((9*H*-Carbazol-3-yl)oxy)-5-chlorophthalonitrile (3). Yield: 1.05 g (60%). FT-IR: cm^{-1} 3406 (N–H), 3079 (Ar–H), 2238 (C≡N), 1120 (C–O–C). ^{1}H NMR (500 MHz, d_6-DMSO): δ/ppm 11.42 (s, 1H), 8.56 (s,1H), 8.22–8.19 (d,1H), 8.15–8.12 (d,1H), 7.61 (s, 1H), 7.51–7.49 (d, 1H), 7.40–7.36 (t, 1H), 7.19–7.16 (t, 1H), 7.19–7.16 (t, 1H), 6.98–6.95 (d,1H). ^{13}C NMR (500 MHz, d_6-DMSO): δ/ppm 158.03, 152.36, 140.99, 140.84, 136.53, 136.53, 128.97, 126.08, 122.52, 122.45, 121.02, 120.63, 119.52, 115.68, 115.51, 115.40, 111.53, 111.33, 109.73, 102.87.

4,5-Bis((9*H*-carbazol-3-yl)oxy)phthalonitrile (4). Yield: 1.70 g (68%). FT-IR: cm^{-1} 3394 (N–H), 3055 (Ar–H), 2236 (C≡N), 1118 (C–O–C). ^{1}H NMR (500 MHz, d_6-DMSO): δ/ppm 11.43 (s, 2H), 8.57 (s, 2H), 8.22–8.20 (d, 2H),8.14–8.12 (d, 2H), 7.62 (s, 2H), 7.50–7.48 (d, 2H), 7.40–7.37 (t, 2H), 7.20–7.16 (t, 2H), 6.98–6.95 (d, 2H). ^{13}C NMR (500 MHz, d_6-DMSO): δ/ppm 158.03, 152.34, 141.02, 136.50, 128.96, 126.07, 122.45, 122.42, 121.03, 120.61, 119.51, 115.66, 115.38, 111.55, 109.70, 102.90.

General procedures for the synthesis of zinc phthalocyanine derivatives (Pc3 and Pc-4)

4-((9*H*-carbazol-3-yl)oxy)-5-chlorophthalonitrile (100 mg, 0.291 mmol) or 4,5-bis((9*H*-carbazol-3-yl)oxy)phthalonitrile (100 mg, mmol) and Zn $(CH_3COO)_2$ {**Pc-3**: (13 mg, 0.072 mmol); **Pc-4**: (9 mg, 0.050 mmol)} were dissolved in DMAE (1.5 mL). The reaction content was stirred at reflux temperature for 24 hours under a nitrogen atmosphere. The content was poured into the ice: water mixture (20 mL) and filtered off. The precipitate was washed with hot *n*-hexane several times and dried in a vacuum oven. The product was purified by applying a column chromatographic technique on silica gel. An *n*-hexane : THF (4 : 1) mixture was used as the eluent.

Compound Pc-3. Yield: 0.055 g (52.50%), mp > 250 °C. FT-IR: cm^{-1} 3423 (N–H), 3051 (Ar–H), 1119 (C–O–C). ^{1}H NMR (500 MHz, d_6-DMSO): δ/ppm 11.39–11.17 (m, 4H), 8.98–7.91 (m, 24H), 7.49–7.35 (m, 12H). MS *m*/*z* calcd for $[M]^+$ 1440.46 found 1436.65 $[M\text{-}4H]^+$. UV-vis (DMSO): λ_{max}/nm^{-1} (log ε) 332 (4.64), 685 (4.94).

Compound Pc-4. Yield: 0.060 g (58%), mp > 250 °C. FT-IR: cm^{-1} 3432 (N–H), 3055 (Ar–H), 1116 (C–O–C). ^{1}H NMR (500 MHz, d_6-DMSO): δ/ppm 11.40 (s, 8H), 8.22–8.20 (d, 4H), 8.15–8.11 (m, 12H), 8.08 (s, 4H), 7.50–7.49 (d, 4H), 7.40–7.36 (t, 8H), 7.27–7.24 (m, 8H), 7.20–7.13 (m, 12H), 7.09 (s, 4H), 6.99–6.95 (d, 8H). MS *m*/*z* calcd for $[M]^+$ 2027.47 found 2074.52 $[M + 2Na + H]^+$. UV-vis (DMSO): λ_{max}/nm^{-1} (log ε) 329 (4.90), 685 (4.76).

Synthesis procedure for compound Pc-6

Silicon(IV) phthalocyanine dichloride (0.100 g, 0.163 mmol) and 2-hydroxycarbazole (0. 060 g, 0.327 mmol) were dissolved in toluene (3 mL, as a solvent). After the addition of sodium hydride (0.020 g, 0.818 mmol), the reaction content was stirred at 130 °C for 48 hours under an inert atmosphere. The solvent was evaporated. The content was washed several times with water and then hot *n*-hexane. The pure product was obtained by performing column chromatography on basic alumina as the stationary phase and THF as the mobile phase. Yield: 0.111 g (75%), mp > 250 °C. FT-IR: cm^{-1} 3416 (N–H), 3063 (Ar–H). ^{1}H NMR (500 MHz, d_6-DMSO): δ/ppm 10.91 (s, 2H), 9.69–9.65 (m, 2H), 8.97–8.93 (m, 8H), 8.50–8.47 (m, 8H), 7.91–7.89 (d, 2H), 7.84–7.81 (d, 2H), 7.36–7.32 (d, 2H), 7.23–7.19 (t, 2H), 7.07–7.02 (t, 2H), 6.86 (s, 2H). MS *m*/*z* calcd for $[M]^+$ 905.03 found 558.16 $[M + CHCA + H]^{2+}$. UV-vis (DMSO): λ_{max}/ nm^{-1} (log ε) 327 (5.00), 682 (4.64).

Preparation of nanoconjugates (Au-Pc-1-6)

Gold nanoparticles[36] and the phthalocyanine-modified gold nanoparticles were prepared according to the procedures that have been extensively explained in the literature.[27,49,50]

Singlet oxygen quantum yield

The singlet oxygen generation capacity of the nanoconjugates (**Au-Pc1-6**) was investigated in DMSO by studying the phosphorescence of singlet oxygen. The spectra were recorded on a Horiba–Jobin–Yvon Fluorimeter with a Hama-matsu NIR PMT 5509.[62] The singlet oxygen quantum yields were determined using the below equation:

$$\varphi_\Delta = \varphi_\Delta(\text{std})\ (\varphi_\Delta \times A(\text{std})/\varphi_\Delta(\text{std}) \times A)$$

where φ_Δ (std) is the singlet oxygen quantum yield of unsubstituted zinc(II) phthalocyanine (ZnPc; φ_Δ = 0.67 in DMSO). φ_Δ is the area under the curve of the peak of singlet oxygen at 1270 nm and *A* is the related absorbance.

Biological studies

DPPH radical scavenging assay

DPPH radical scavenging activities of the nanoconjugates (**Au-Pc-1-6**) were investigated according to the method extensively described in Ref. 75. Trolox was utilized as the standard. 0.15 mL of DPPH (0.1 mM in methanol) was added to 0.15 mL of the prepared nanoconjugate solution (in DMSO). The solution was kept in the dark for 50 min. The absorbance change was studied at 517 nm using a UV–visible spectrophotometer (Spectra max-384, USA). All the determinations were carried out three times. SC_{50} (mg compound per mL) is the concentration of the samples which causes 50% scavenging of the DPPH radical. This value was used for the expression of the radical scavenging activities of the nanoconjugates.

Cell culture and MTT assay

The anticancer activities of nanoconjugates (**Au-Pc-1-6**) against DLD-1 (human colon adenocarcinoma cell line) and HepG2 (hepatocellular carcinoma cell line) were examined in this study. Cells were cultured in high glucose DMEM supplemented with 10% FBS, 1% penicillin-streptomycin, and 1% L-glutamine. Then, the cells were maintained at 37 °C in a 5% CO_2 humidified incubator. The cells were cultured in 75 cm^2 flasks. As the cells reached 80% confluence, they were seeded in 96 well plates as 5×10^3 cells per well.

Different concentrations of the nanoconjugates ranging from 12.5 to 200 μM were exposed to three cell lines in triplicate wells. Cisplatin was used as a positive control whereas the non-treated cells were utilized as a control group. Then, the plates were divided into two groups. The darkness group was maintained under normal culture conditions; however, the white light group was incubated for 1 hour under normal conditions and then exposed to white light (3000 l×) for 2 hours. The distance between the plate surface and the light source was 4 cm. Furthermore, the plates were kept under normal incubation conditions for 24 hours. The MTT solution (0.5 mg mL^{-1} in DPBS) was added to the wells. After 3 hours, the wells' contents were extracted and 100 μL of DMSO was added to dissolve formazan crystals. The plates were monitored between 560 and 750 nm using an ELISA reader (Glomax, Promega, USA). The half-maximal inhibitory concentration (IC_{50}) was calculated by applying the obtained optical density (OD) values. Statistical evaluation was carried out by performing a *T*-Test.

Conclusions

In this study, two new phthalonitriles and their zinc(II) phthalocyanines were synthesized and characterized. Also, their non-peripherally tetra-substituted and peripherally tetra-substituted zinc(II) phthalocyanines were prepared along with axially di-substituted silicon(IV) phthalocyanine to compare the influence of the metal ions and phthalocyanine periphery on the biological features of carbazole-containing phthalocyanines. All the nanoconjugates exhibited acceptable singlet oxygen generation abilities for photodynamic therapy. The presence of carbazole groups at the axial positions of the silicon(IV) phthalocyanine led to the higher efficiency of singlet oxygen production. Although the antioxidant activities of the phthalocyanines were significantly affected by the position and number of substituents, their DNA cleavage activities were almost assigned to the positions of the ligands. The *in vitro* cytotoxic properties of the newly synthesized phthalocyanine–gold nanoconjugates were examined against DLD-1 and HepG2 cell lines by applying an MTT assay. The obtained results indicated that all the nanoconjugates exhibited cytotoxic and phototoxic activities against the studied cell lines. Nanoconjugates **Au-Pc2**, **Au-Pc3**, **Au-Pc5**, and **Au-Pc6** displayed statistically different phototoxic effects under white light irradiation compared to those in the dark. The cytotoxic and phototoxic features of the nanoconjugates were affected by the irradiation time (48 and 72 hours) and a power source. Since all the studied nanoconjugates displayed high cytotoxic and phototoxic effects, they can be utilized as chemotherapeutical/photodynamic agents after further investigations. The highest IC_{50} values were obtained for nanoconjugate **Au-Pc6**. Particularly, this nanoconjugate exhibited high activity the same as that of Cisplatin against the human cancer cell line (DLD-1).

Conflicts of interest

There are no conflicts to declare.

Acknowledgements

This work was supported financially by the Scientific and Technological Research Council of Türkiye (TUBITAK; 122Z036). Zehra Altuntaş Bayır appreciates the funding by Research Fund of the Istanbul Technical University. (Project Number: THD-2022-44090).

References

1 H. Fu, H. Wu, X. Hou, F. Xiao and B. Shao, *Synth. Met.*, 2006, **156**, 809.
2 C. Ito, M. Itoigawa, K. Aizawa, K. Yoshida, N. Ruangrungsi and H. Furukawa, *J. Nat. Prod.*, 2009, **72**, 1202.
3 A. C. Adebajo, E. O. Iwalewa, E. M. Obuotor, G. F. Ibikunle, N. O. Omisore, C. O. Adewunmi, O. O. Obaparusi, M. Klaes, G. E. Adetogun, T. J. Schmidt and E. J. Verspohl, *J. Ethnopharmacol.*, 2009, **122**, 10.
4 Q. Ma, J. Tian, J. Yang, A. Wang, T. Ji, Y. Wang and Y. Su, *Fitoterapia*, 2013, **87**, 1.
5 J. Wang, Y. Zheng, T. Efferth, R. Wang, Y. Shen and X. Hao, *Phytochemistry*, 2005, **66**, 697.
6 T. Nakamura, N. Kodama, Y. Arai, T. Kumamoto, Y. Higuchi, C. Chaichantipyuth, T. Ishikawa, K. Ueno and S. Yano, *J. Nat. Med.*, 2009, **63**, 21.
7 C. Asche, W. Frank, A. Albert and U. Kucklaender, *Bioorg. Med. Chem.*, 2005, **13**, 819.
8 Y. Hajbi, C. Neagoie, B. Biannic, A. Chilloux, E. Vedrenne, B. Bladeyrou, C. Bailly, J. Y. Mérour, S. Rosca, S. Routier and A. Lansiaux, *Eur. J. Med. Chem.*, 2010, **45**, 5428.
9 S. Achab, K. Diker and P. Potier, *Tetrahedron Lett.*, 2001, **42**, 8825.
10 H. J. Lee, G. Schaefer, T. P. Heffron, L. Shao, X. Ye, S. Sideris, S. Malek, E. Chan, M. Merchant, H. La, S. Ubhayakar, R. L. Yauch, V. Pirazzoli, K. Politi and J. Settleman, *Cancer Discovery*, 2013, **3**, 168.
11 Z. Bouaziz, S. Issa, J. Gentili, A. Gratz, A. Bollacke, M. Kassack, J. Jose, L. Herfindal, G. Gausdal, S. O. Døskeland, C. Mullie, P. Sonnet, C. Desgrouas,

 This journal is © The Royal Society of Chemistry 2023

N. Taudon, G. Valdameri, A. Di Pietro, M. Baitiche and M. Le Borgne, *J. Enzym. Inhib. Med. Chem.*, 2015, **30**, 180.
12 B. Tylinska, R. J. Howorko, H. Mastalarz, D. Klopotowska, B. Fillip and J. Wietrzyk, *Acta Pol. Pharm. Drug Res.*, 2010, **67**, 495.
13 J. D. Ha, S. K. Kang, H. G. Cheon and J. K. Choi, *Korean Chem. Soc.*, 2004, **25**, 1784.
14 H. Chabane, C. Lamazzi, V. Thiery, G. Guillaumet and T. Besson, *Tetrahedron Lett.*, 2002, **43**, 2483.
15 A. E. Martin and K. J. R. Prasad, *Acta Pharm.*, 2006, **56**, 79.
16 M. Göksel, İ. F Sengul, H. Kandemir and M. Durmuş, *J. Porphyrins Phthalocyanines*, 2016, **20**, 708.
17 R. Olgac, T. Soganci, Y. Baygu, Y. Gök and M. Ak, *Biosens. Bioelectron.*, 2017, **98**, 202.
18 S. Çol, M. Emirik, Z. Alım and A. Baran, *Appl. Organomet. Chem.*, 2022, **36**, e6799.
19 C. C. Leznoff and A. B. P. Lever, *Phthalocyanines Properties and Applications*, VCH, New York, 1996, pp. 1–4.
20 Ö. Bekaroğlu, *Appl. Organomet. Chem.*, 1996, **10**, 605.
21 Z. A. Bayır, *Dyes Pigm.*, 2005, **65**, 235–242.
22 O. İpsiz, H. Y. Yenilmez, K. Kaya, A. Koca and Z. A. Bayır, *Synth. Met.*, 2016, **217**, 94.
23 E. Kaplan, T. Karazehir, S. Gümrükçü, B. Sarac, A. S. Sarac and E. Hamuryudan, *Mol. Syst. Des. Eng.*, 2023, DOI: **10.1039/D2ME00191H**.
24 R. Diaz-Torres and S. Alvarez, *Dalton Trans.*, 2011, **40**, 10742.
25 M. Moeini Alishah, H. Y. Yenilmez, İ. Özçeşmeci, B. Ş Sesalan and Z. A. Bayır, *Turk. J. Chem.*, 2018, **42**, 572.
26 H. P. Karaoğlu, Ö. Sağlam, S. Özdemir, S. Gonca and M. B. Koçak, *Dalton Trans.*, 2021, **50**, 9700–9708.
27 S. D'Souza, P. Mashazi, J. Britton and T. Nyokong, *Polyhedron*, 2015, **99**, 112.
28 H. Y. Yenilmez, B. Ustamehmetoğlu, E. Sezer and Z. A. Bayır, *J. Solid State Electrochem.*, 2018, **22**(2), 505.
29 M. Özçeşmeci, İ. Özçeşmeci, İ. Sorar and E. Hamuryudan, *Inorg. Chem. Commun.*, 2017, **86**, 209.
30 A. Kalkan, A. Koca and Z. A. Bayır, *Polyhedron*, 2004, **23**(18), 3155.
31 G. Obaid, I. Chambrier, M. J. Cook and D. A. Russell, *Angew. Chem., Int. Ed.*, 2012, **51**, 6158.
32 T. Stuchinskaya, M. Moreno, M. J. Cook, D. R. Edwards and D. A. Russell, *Photochem. Photobiol. Sci.*, 2011, **10**, 822.
33 E. C. Dreaden, M. A. Mackey, X. Huang, B. Kang and M. A. El-Sayed, *Chem. Soc. Rev.*, 2011, **40**, 3391.
34 E. E. Connor, J. Mwamuka, A. Gole, C. J. Murphy and M. D. Wyatt, *Small*, 2005, **1**, 325.
35 J. Panyam, M. M. Dali, S. K. Sahoo, W. Ma, S. S. Chakravarthi, G. L. Amidon, R. J. Levy and V. Labhasetwar, *J. Controlled Release*, 2003, **92**, 173.
36 J. Abolhasani and N. Farajzadeh, *Luminescence*, 2015, **30**(3), 257.
37 R. Bhattacharya and P. Mukherjee, *Adv. Drug Delivery Rev.*, 2008, **60**, 1289.
38 T. P. Mthethwa, Y. Arslanoglu, E. Antunes and T. Nyokong, *Polyhedron*, 2012, **38**(1), 169–177.
39 Y. Cheng, A. Samia, J. D. Meyers, I. Panagopoulos, B. Fei and C. Burda, *J. Am. Chem. Soc.*, 2008, **130**(32), 10643–10647.
40 V. Amendola, G. Mattei, C. Cusan, M. Prato and M. Meneghetti, *Synth. Met.*, 2005, **155**(22), 283–286.
41 D. Demirkapı, A. S. irin, B. Turanlı-Yıldız, Z. P. Çakar and B. S.- Sesalan, *Synth. Met.*, 2014, **187**, 152–159.
42 F. Shahidi and Y. Zhong, Lipid oxidation: Measurement methods, in *Bailey's industrial oil and fat products*, ed. F. Shahidi, John Wiley & Sons, Inc, Hoboken, NJ, 6th edn., 2005, vol. 1, pp. 357–386.
43 K. B. Beckman and B. N. Ames, The free radical theory of aging matures, *Physiol. Rev.*, 1998, **78**, 547.
44 F. Shahidi, *Die Nahrung.*, 2000, **44**, 158.
45 W. Song, C. M. Derito, K. M. Liu, X. He, M. Dong and R. H. Liu, *J. Agric. Food Chem.*, 2010, **58**, 6621.
46 K. L. Wolfe and R. H. Liu, *J. Agric. Food Chem.*, 2007, **55**, 8896.
47 N. O. Yakimovich, A. A. Ezhevskii, D. V. Guseinov, L. A. Smirnova, T. A. Gracheva and K. S. Klychkov, *Russ. Chem. Bull.*, 2008, **57**(3), 520.
48 N. Farajzadeh, S. Özdemir, G. Tollu, Z. A. Bayır and M. B. Koçak, *J. Inorg. Biochem.*, 2022, **234**, 111888.
49 N. Farajzadeh, J. Aftab, H. Y. Yenilmez, S. Özdemir, S. Gonca and Z. A. Bayır, *New J. Chem.*, 2022, 5374.
50 J. Aftab, N. Farajzadeh, H. Y. Yenilmez, S. Özdemir, S. Gonca and Z. A. Bayır, *Dalton Trans.*, 2022, **51**, 4466.
51 A. Kamal, R. Ramu, V. Tekumalla, G. B. R. Khanna, M. S. Barkume, A. S. Juvekarb and S. M. Zingde, *Bioorg. Med. Chem.*, 2007, **15**, 6868.
52 R. A. Weinberg, *Scientific America, Special issue: What you need to know about cancer*, 1996, 275((3)), 62.
53 S. Raniolo, S. Croce, R. P. Thomsen, A. H. Okholm, V. Unida, F. Iacovelli, A. Manetto, J. Kjems, A. Desideri and S. Biocca, *Nanoscale*, 2019, **11**, 10808.
54 H. H. Thorp, *J. Inorg. Organomet. Polym.*, 1993, **3**, 111.
55 A. M. Pyle and J. K. Barton, *Prog. Inorg. Chem.*, 1990, **38**, 413.
56 S. Lippard, *J. Acc. Chem. Res.*, 1978, **11**(5), 211.
57 P. Khoza, E. Antunes and T. Nyokong, *Polyhedron*, 2013, **61**, 119.
58 P. Khoza, E. Antunes and T. Nyokong, *Dyes Pigm.*, 2014, **104**, 57.
59 S. A. Majeed, K. E. Sekhosana and A. Tuhl, *Arabian J. Chem.*, 2020, **13**(12), 8848.
60 O. M. Bankole and T. Nyokong, *J. Mol. Struct.*, 2017, **1136**, 309.
61 J. E. V. Lier and D. Kessel, *Photodynamic Therapy of Neoplastic Diseases*, CRC Press, Boca Raton, FL, 1990, vol. 1.
62 F. Wilkinson and A. Ross, *J. Phys. Chem. Ref. Data*, 1992, **22**, 113.
63 V. Çakır, M. Go ksel, M. T. Durmus- and Z. Biyiklioglu, *Dyes Pigm.*, 2016, **125**, 414–425.
64 E. H. Alici, A. Günsel, M. Akin, A. T. Bilgiçli, G. Arabaci and M. N. Yarasir, *J. Coord. Chem.*, 2018, **71**(19), 3077.

65 M. H. Salehi and A. R. Karimi, *Polym. Degrad. Stab.*, 2018, **151**, 105.
66 G. G. Çelik, S. Gonca, B. Şahin, S. Özdemir, D. Atilla and A. G. Gürek, *Dalton Trans.*, 2022, **51**, 7517.
67 M.-H. Hsu, T. Josephrajan, C.-S. Yeh, D.-B. Shieh, W.-C. Su and J. R. Hwu, *Bioconjugate Chem.*, 2007, **18**, 1709.
68 B. Barut, C.Ö Yalçın, Ü. Demirbaş, H. T. Akçay, H. Kantekin and A. Ozel, *J. Mol. Struct.*, 2020, **1218**, 128502.
69 M. Ozdemir, G. O. Artuc, E. M. Guler, B. Yalcin, U. Salan, K. Bozali, A. O. Gorgulu and M. Bulut, *Dyes Pigm.*, 2021, **196**, 109832.
70 N. W. Nkune, C. A. Kruger and H. Abrahamse, *Adv. Anticancer Agents Med. Chem.*, 2021, **21**, 137.
71 H. Y. Yenilmez, N. Farajzadeh, N. G. Kuşçulu, D. Bahar, S. Özdemir, G. Tollu, M. Güllü and Z. A. Bayır, *Chem. Biodivers.*, 2023, DOI: **10.1002/cbdv.202201167**.
72 X.-Q. Zhou, L.-B. Meng, Q. Huang, J. Li, K. Zheng, F.-L. Zhang, J.-Y. Liu and J.-P. Xue, *ChemMedChem*, 2015, **10**, 304.
73 A. Sowa, A. Höing, U. Dobrindt, S. K. Knauer, A. Galstyan and J. Voskuhl, *Chem. – Eur. J.*, 2021, **27**, 14672.
74 P.-C. Lo, J.-D. Huang, D. Y. Y. Cheng, E. Y. M. Chan, W.-P. Fong, W.-H. Ko and D. K. P. Ng, *Chem. – Eur. J.*, 2004, **10**(19), 4831.
75 P. Molyneux, *Songklanakarin J. Sci. Technol.*, 2004, **26**(2), 211.

This journal is © The Royal Society of Chemistry 2023